Stator Winding Internal Thermal Monitoring and Analysis Using *In Situ* FBG Sensing Technology

Anees Mohammed, *Student Member, IEEE*, and Siniša Djurović, *Member, IEEE*

***Abstract*—This paper reports a novel thermal monitoring scheme for on-line internal temperature measurement in low-voltage random wound machine stator windings. The scheme is based on utilizing electrically nonconductive and electromagnetic interference immune fiber optic sensing technology embedded in close proximity of hot spots of interest to create a robust distributed thermal monitoring network within the machine windings. The key design and implementation features of the proposed system are presented and applied on a prototype mains-fed induction motor. The on-line thermal monitoring performance is examined in a number of typical continuous and periodic running duty tests, as defined by the relevant IEC standards for rating and performance of rotating electrical machines. It is shown that the presented scheme has the potential to provide competent on-line measurement of critical machine thermal hot spots that are largely beyond the effective reach of conventional thermal monitoring solutions. Furthermore, the proposed scheme underpins a higher fidelity understanding of the distribution and propagation of winding thermal stress, demonstrated by the experimental analysis reported in the paper.**

***Index Terms*—Induction motor, on-line thermal monitoring, internal stator winding temperature, FBG sensor.**

I. Introduction

LOW voltage random wound electrical machines (LVEMs) are currently finding increased use in novel, safety critical energy conversion system applications, such as those in aerospace, electric vehicle and offshore wind industries [1]–[3]. These industrial applications impose increasingly higher requirements for reliability and performance of the employed electrical machines. As thermal stress is the major contributor to lifetime and performance reduction of LVEMs and reliable understanding of machine thermal conditions a precursor to achieving more effective machine exploitation, the area of machine thermal monitoring and analysis is receiving increased attention [4]–[7]. Development and application of improved thermal monitoring techniques that can enable performance advances through increased awareness of operational stresses and enhanced thermal management is highly relevant in this respect [8], [9].

Manuscript received October 3, 2017; revised January 19, 2018; accepted April 9, 2018. Date of publication April 18, 2018; date of current version August 17, 2018. This work was supported by the UK Engineering and Physical Sciences Research Council HOME-Offshore: Holistic Operation and Maintenance for Energy from Offshore Wind Farms Consortium under Grant EP/P009743/1. Paper no. TEC-00759-2017. (*Corresponding author: Siniša Djurović.*)

The authors are with the School of Electrical and Electronic Engineering, University of Manchester, Manchester M13 9PL, U.K. (e-mail: Anees.mohammed@postgrad.manchester.ac.uk; Sinisa.Durovic@manchester.ac.uk).

Color versions of one or more of the figures in this paper are available online at http://ieeexplore.ieee.org.

Digital Object Identifier 10.1109/TEC.2018.2826229

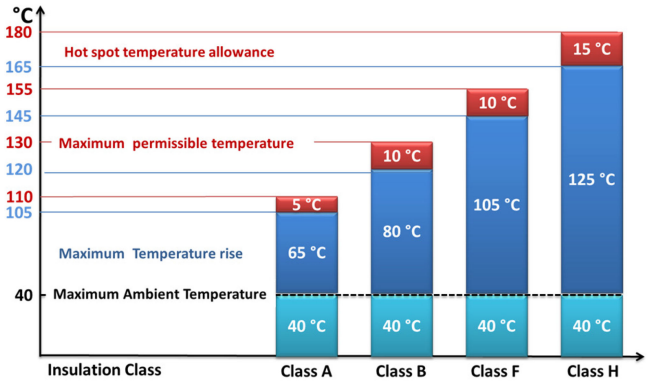

Fig. 1. Thermal limits for insulation classes A, B, C, and F [14].

Thermal stress such as that occurring in overheating or cycling transients degrades the integrity of the winding organic insulation material, the machine component most susceptible to thermal stress. This results in its accelerated thermal aging: the ensuing insulation deterioration eventually leads to machine failure [10]. Thermal monitoring is thus a fundamental requirement for machine protection and enhancement of its reliability [11]. This is particularly pertinent where the internal thermal stress conditions in windings are concerned, as these are invariably the points of highest temperature within the machine: winding thermal hot spots are in slot centers and end-windings interior, their distribution depending on machine design and cooling arrangements. The allowable temperature in windings is defined by the thermal limits within which their insulation material retains its mechanical and electrical integrity to enable fault-free machine operation [12], [13]. The relevant standards identify machine insulation classes by their maximum allowable operating temperature while in service [14]: for a given insulation class, the maximum allowable temperature is defined as the sum of the ambient temperature (max 40 °C), the permissible temperature rise (i.e the difference between ambient temperature and the final elevated temperature) and the hot spot allowance temperature, as illustrated in Fig. 1. The hot spot allowance temperature provides a thermal safety margin for the temperature of the winding interior; this is typically the point of highest temperature in the winding which is usually challenging to directly measure or estimate due to limitations of the available measurement methods [15]. Accurate knowledge of winding hotspot temperature of an in-service machine would enable cooling system control directly related to hot spot temperature and thus machine lifetime extension through hot

spot regulation. This would also enable performance improvements through controlled overloads or identification of overly conservative ratings, and be used for correction of temperature dependent machine model parameters to increase automation performance [4], [7].

The current practice for monitoring winding thermal conditions is based on employing temperature estimation techniques or embedded thermal sensors [16]. The former are generally established using a thermal model-based or a parameter-based temperature estimator [17]–[19]. Assessing winding temperature using a parameter-based temperature estimator is achieved by estimating on-line the winding electrical resistance and hence its temperature [18]. However this cannot provide a full thermal image of the winding nor its hot spots and yields only the average winding temperature, while also being limited in accurate tracking of thermal change during fast transient conditions [10]. Hot spot on-line monitoring using thermal model-based estimators such as finite element (FE) or lumped network models imposes considerable constraints: the FE models are computationally demanding and therefore not effective in on-line applications, while lumped network thermal models impose complexity in appropriate evaluation of model parameters including parameter dependency on thermal conditions [18], [19].

Winding thermal hot spot monitoring using conventional sensing techniques such as thermocouples (TCs) or resistance temperature detectors (RTDs) can be limited for safety critical applications, primarily due to inherent use of electrically conductive material in the sensor structure: this poses a risk to the winding and the sensing system integrity, as any direct contact between the sensor and the winding can allow high current flow. Insulating these sensors with appropriate packaging can minimise this risk. This however considerably increases the sensor structure size, which can be impractical where the machine geometries of interest for monitoring such as the slot areas are concerned, and can compromise vital design parameters [20]. As a consequence of the constraints imposed by the winding construction and the sensor structure and its wiring, the sensing points in which TC and RTD sensors are applied in LVEMs are typically on end-windings and more rarely on winding surface of the slot section, and not in the winding centre where the highest temperature is located [21], [22]. Further general constraints to more effective RTD and TC application in safety critical electrical machinery are imposed by their intrinsic low electromagnetic interference (EMI) immunity and low resistance to harsh environmental conditions and long term deployment [23].

The existing thermal monitoring techniques are limited in safe and accurate monitoring of the highest temperature points in LVEMs. The availability of reliable thermal monitoring tools, able to accurately track winding hotspot temperatures in all possible operating conditions will be essential in meeting the desired LVEM improved efficacy usage targets in future system critical transport and industrial sectors applications. A thermal sensing alternative is provided by recent advances in fibre-optic fibre Bragg grating (FBG) sensing technology, whose inherent robustness, flexibility, long lifetime, electrical/EMI immunity, multiplexing and small size make it an attractive candidate for improving embedded thermal monitoring solutions for machine wound components [24]. The FBG sensor cost is currently comparable to cost of TC and RTD sensors conventionally used in electric machine applications, but the required FBG interrogator systems are costly. However, FBG sensing features can provide a number of attractive monitoring and performance improvements in electric machines that would be very challenging to deliver by alternative sensing or design approaches. In addition, the inherently multi-physical and multiplexing nature of FBG sensing systems has the potential to provide a sizeable considerable reduction of the overall monitoring system size and cost [25]–[27]. Despite its current relatively high cost, this sensing technology has already found use in aerospace and wind industries where its features have contributed to development of more effective monitoring systems [28]–[30]. The use of these sensors for hot spot monitoring in in-service LVEMs presents an attractive opportunity but still remains largely unexplored.

The interest in applying FBG sensors in electric machinery for mechanical and thermal measurements has been increasing recently [31]–[35]. FBG sensors are now identified as a suitable thermal monitoring technique for thermal cycle testing of bars and coils of large rotating machines, as specified by the IEEE 1310-2012 standard [36]. The general FBG potential for thermal monitoring internal to machine structure is assessed in [24], [32], [33] for low and high power machinery. The reported literature however focuses on large form wound winding structures [24], [32] and winding surface [33] thermal monitoring in LVEMs, and does not consider coil embedded hot spot locations that are of critical interest. In addition, the FBG thermal sensor packaging designs used in reported studies utilise conductive materials such as stainless steel and aluminium which can impose operational challenges in safety critical machine applications. Advances have recently been made in understanding the optimal features of random wound coil embedded FBG thermal sensors use for in-situ monitoring of hot spot temperature [37]–[40]. This was however done only on prototype IEEE motorette systems and its application and performance in operating machines is yet to be examined.

This study reports an in-situ FBG thermal sensing technique for on-line thermal monitoring of the stator winding internal temperature in widely used random wound squirrel cage induction motors. The proposed technique enables adequate real-time monitoring of stator winding hot spot temperatures, in locations that are largely beyond effective reach of conventional thermal monitoring in practical machine applications. The reported scheme is evaluated on a commercial totally enclosed fan cooled (TEFC) induction machine design. The test motor was rewound for the purpose of proposed scheme application and then operated in mains supplied conditions under dynamic thermal cycles defined by the relevant IEC standard [23]. The obtained measurements are cross-correlated with predictions from a representative FE thermal model [41]–[44] to further investigate the potential and performance of the presented scheme. The proposed system's on-line monitoring performance was found to deliver an acceptable indication of the winding hot spot temperatures in a range of typical dynamic operating regimes.

TABLE I
TEST MOTOR SPECIFICATION

TEFC Motor Data	
Rated Power / Voltage / Current	0.55 kW / 400 V / 1.6A
Efficiency	66 %, IE1
Rated speed	1380 rpm
Pole number	4
Cooling method	IC 41
Slot number stator / rotor	24 / 30
Insulation class	F
Temperature rise class	B
Duty cycle type rating	S1
Frame / Core axial length	130 / 80 mm
Housing diameter	110 mm
Design standard	IEC 60034

II. THERMAL HOT SPOT IDENTIFICATION

This study focuses on development of a winding hot spot in-situ thermal monitoring system, as a means of improving the attainable on-line thermal monitoring. In addition to sensing technique improvement an essential element in providing enhanced monitoring is the reliable identification of sensor placement points. These ideally need to be in, or close to, positions of highest temperature in wound components to ensure the monitoring system reports the maximum existing thermal stress. To this end and for illustration purposes, the hot spot locations in the investigated commercial TEFC motor were first examined using thermal simulation.

A. Thermal Model Study

The studied motor specification is presented in Table I. A thermal model of the test motor was developed using the Motor-CAD software package for thermal analysis [41]. Motor-CAD provides a specialised tool for design and analysis of thermal aspects in electrical machines [42], [44]; its machine thermal models are based on an analytical lumped parameter thermal network enhanced with numerical 2D FE analysis for steady-state solutions. The integrated FE analysis provides increased detail on conduction heat transfer in various components in the motor, which allows the prediction of hot spot temperatures in the machine structure. The test motor thermal model in Motor-CAD was developed using detailed geometry/design data and material properties of the examined motor. The motor losses required for model development were obtained based on the procedure prescribed by the IEEE 112 standard [45]. The model was optimised using DC power, locked rotor and load tests [41], [44], [46].

Development of a representative winding thermal model for random wound electrical machines is challenging due to the random distribution of winding conductors in the slot and end-winding portions. For the purpose of winding thermal model development its structure can be divided into three portions: the non-drive end end-winding, the slot winding and the drive end end-winding. For the slot winding portion a thermal slot model representation that allows the conductors to be arbitrarily

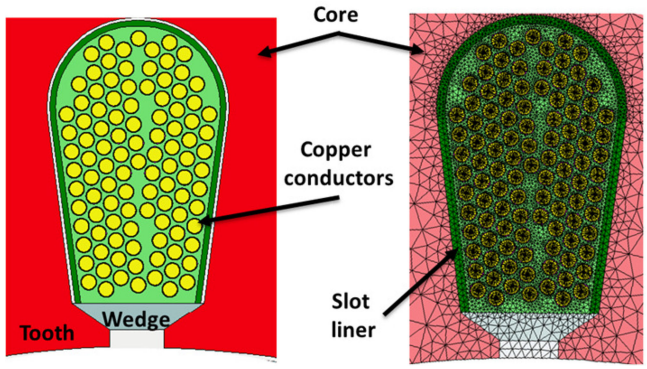

Fig. 2. Stator slot thermal model.

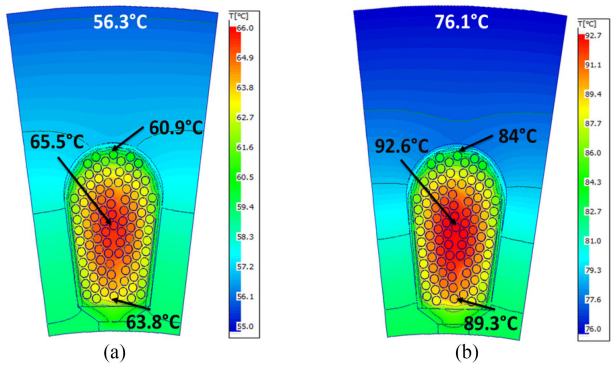

Fig. 3. Predicted steady-state temperature gradient of the slot section. (a) No-load. (b) Full-load.

positioned in the slot and considers other slot components such as slot liner, wedges and impregnation is used in this work. Fig. 2 shows the details of the slot thermal model for the examined TEFC motor. The end-windings model is more complex as their structure is inherently random and the heat convection of the external end-winding surface plays a significant role. In this study an end-winding portion is modelled as a single thermal component based on its available shape and volume data.

To enhance the thermal prediction of the end and slot winding portions the total stator winding loss was divided between portions based on their length [41]:

$$P_{slot} = P_s * \frac{(2\ x\ stator\ axial\ lenght)}{(2\ x\ stator\ axial\ lenght + Ewd\ lenght)}, \quad (1)$$

$$P_{Ewd} = P_s * \frac{(\ Ewd\ lenght)}{(2\ x\ stator\ axial\ lenght + Ewd\ lenght)}, \quad (2)$$

where: P_s is the total stator winding copper loss, P_{slot} and P_{Ewd} are the copper loss in the slot and end-winding portions respectively, *stator axial length* represents the coil axial length in the slot portion and the *Ewd length* represents the coil ends length in the drive end (DE) and non-drive end (NDE) end-windings. The total calculated end-winding loss is evenly divided between DE and NDE end-windings.

Figs. 3 and 4 show the predicted winding steady-state temperature of the examined TEFC motor at no-load and full- load

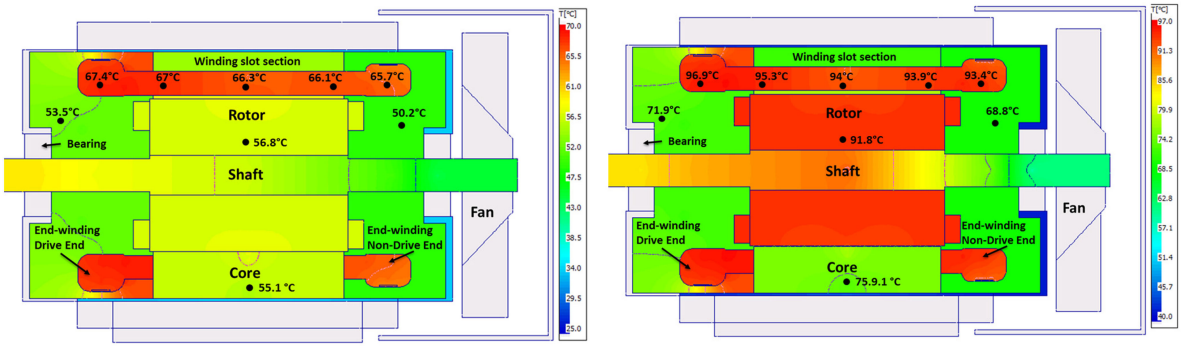

Fig. 4. Predicted axial thermal gradient in the test motor. (a) No-load. (b) Full-load.

conditions. Fig. 3 shows the temperature distribution of the winding slot section. This is presented for one slot only as, for the sake of the model study, all slots are assumed to have identical conductor distribution and the calculated slot copper loss from (1) is evenly distributed between individual stator slots. As is generally expected, the predicted slot winding portion hot spot temperature is located in the centre of the slot. The predicted slot hot spot temperature increases from ≈65.5 °C at no-load to ≈92.6 °C at full-load. The predicted difference between the maximum and minimum temperature within the slot section is ≈4.5 °C at no-load increasing to ≈8 °C at full-load. The bottom of the slot is the coolest part of the slot section, as it is highly affected by the stator iron yoke.

The predicted temperature gradients in the axial cross section of the examined TEFC motor at no-load and full-load conditions are shown in Fig. 4. It is apparent that the motor winding temperature gradually increases with distance from the cooling fan, as is normally anticipated. For the examined motor design the hottest temperature in the axial cross section was predicted in the DE end-winding at ≈67.4 °C and ≈96.9 °C at no-load and full-load conditions, respectively. The predicted temperatures in DE end-winding were ≈1.7 °C and ≈3.5 °C higher than in NDE end-windings at no-load and full-load conditions, respectively. For the slot axial section, the hottest location is displaced towards the core drive end, as is generally expected for a non-drive end fan cooled machine. The maximum and minimum predicted temperatures in the slot axial section are ≈67 °C and ≈66.1 °C at no-load and ≈95.3 °C and ≈93.9 °C at full-load. This results in a maximum temperature difference along the slot axial length section of ≈1.4 °C. The axial thermal change effects in the slot section are seen not to be considerable, as would be expected of the examined relatively small size machine design. However, this thermal difference is highly dependent on and varies with motor thermal design and size.

B. Thermal Monitoring Point Requirements

The thermal model predictions clearly show that, as is generally expected, the highest hot spot temperature in the examined motor is in its DE end-windings followed by that in the centre of the winding slot portions. Monitoring only the highest thermal hot spot located in the DE end-windings however does not provide sufficient understanding of the existing thermal conditions in the motor. This stems from the fact that the end-winding portions combine the coils of all phase windings into a single thermal component. In abnormal operating conditions, such as for example a supply or other inherent electrical unbalance, different current levels can exist in different phase windings resulting in unevenly distributed coper loss across phases and thus an uneven temperature between individual phase windings. The temperature measured in the end-windings is the average temperature of the separate phase winding coils comprising it, and does not enable the understanding of existing thermal conditions in individual phases, which may in this case exceed the temperature levels observed in the end-winding. The same is valid for operation under electric fault conditions such as inter-turn faults, where high current and therefore thermal stress can typically be localised within a few turns of a single, faulty, phase winding. It is evident that monitoring the slot hotspot temperature in these conditions can provide more accurate information on the actual thermal status of individual phase windings. However, monitoring only the slot portion hot spot thermal conditions would ignore the temperature rise in the DE end-winding due to its slow cooling process caused by its distance from the cooling fan and would therefore not be appropriate. The optimum solution is therefore to design the thermal monitoring system to observe both end-winding and slot portion hot spots in all machine operating conditions; this requires thermal sensors that are suitable for effective application in a variety of slot and end-winding centre positions within the motor geometry.

III. FBG Sensing Principles and In-Situ Monitoring System Design

A. FBG Temperature Sensor Operating Principles

FBGs are the periodic gratings on the optical fibre core that result in a periodic modulation of its refractive index when exposed to an interference pattern of laser light [47]. The wavelengths reflected by the FBG structure will alter with the variation in the strain and/or temperature it is exposed to, thus enabling the fibre structure to act as a strain and thermal excitation sensitive element. With appropriate design [37]–[40] this phenomenon enables the grated fibre to be utilised as an

exclusively mechanical or a thermal sensor. The reflected FBG wavelength is known as the Bragg (i.e., centre) wavelength, λ_B , and is defined by [47]:

$$\lambda_B = 2\,\Lambda\, n_{eff} \tag{3}$$

where: Λ is the grating period (i.e., the spacing between successive gratings) and n_{eff} is the effective fibre core refractive index. A change in the fibre temperature and/or strain will give rise to a change in n_{eff} and Λ, and consequently result in an alteration of the reflected wavelength. The reflected Bragg wavelength relative rate of change can be defined in terms of the existing thermal and/or mechanical excitation as [48]:

$$\Delta\lambda_B = \overbrace{2\left(\Lambda\frac{dn_{eff}}{d\varepsilon} + n_{ef}\frac{d\Lambda}{d\varepsilon}\right)\Delta\varepsilon}^{A} + \overbrace{2\left(\Lambda\frac{dn_{eff}}{dT} + n_{ef}\frac{d\Lambda}{dT}\right)\Delta T}^{B} \tag{4}$$

where: ε is strain and T is temperature. Term A in (4) represents Bragg wavelength shift caused by the strain induced elastic-optic effect, while term B describes the temperature change induced wavelength shift that arises due to thermo-optic and thermal expansion effects [47]. The reflected wavelength variation due to temperature change only can be expressed in terms of the fibre thermal characteristics as [49]:

$$\Delta\lambda_B = \lambda_B\,(\alpha + \xi)\,\Delta T. \tag{5}$$

where: α is the fibre thermal expansion coefficient ($\approx$0.55 $\times$ 10^{-6}/°C) and ξ is the fibre thermo-optic coefficient ($\approx$6.67 $\times$ 10^{-6}/°C) [47]. For a standard bare FBG with the Bragg wavelength of 1550 nm operating at ambient temperature the fibre thermal sensitivity is $\approx$11 pm/°C [48].

B. In-Situ FBG Temperature Sensor Design

The target sensing application in this study is internal thermal monitoring within a random wound stator winding structure in a class F insulated electrical machine, in direct proximity to the winding thermal hot spots located in the coil centre. The primary design constraints of the thermal sensing system, arising from its application within a current carrying coil, are the desirability for the sensing element to be electrically non-conductive and EMI immune with a size sufficiently small to enable seamless sensor implantation in the target hot spot position between individual current carrying conductors, without significant disturbance of the designed motor slot fill factor. In addition, the sensing element has to be capable to operate in and withstand the thermal environment characteristic of the examined conventional class F insulated machine design.

FBG sensing fibres are inherently immune to EMI, non-conductive and typically manufactured in diameter sizes of a few micro meters. An individual fibre is extremely fragile and requires suitable packaging to protect its mechanical integrity. Another important role of packaging in exclusively thermal sensing applications is to isolate the sensing fibre from mechanical excitation and ensure a sensor design that is only

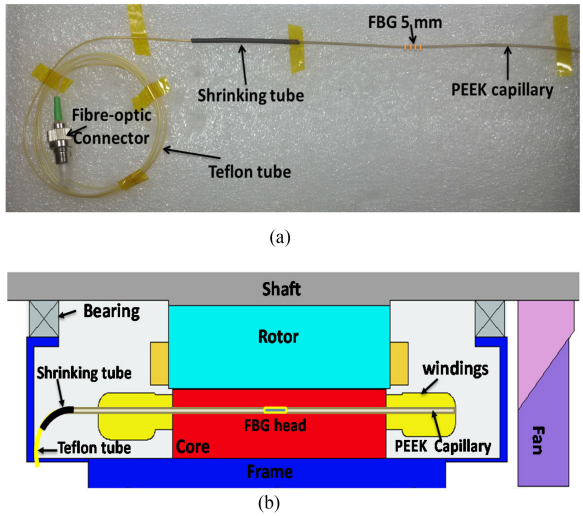

Fig. 5. FBG sensor for in-situ hot spot temperature monitoring. (a) Sensing probe design. (b) In-situ FBG sensor installation.

temperature sensitive [37]. To satisfy the said design constraints a Polyetheretherketon (PEEK) capillary is used in this work to package the FBG sensing heads. PEEK was chosen due to its dielectric and mechanical properties; it has a thermal conductivity of 0.173 W/m.k and can withstand operating temperatures in excess of $\approx$250 °C [38].

Fig. 5(a) shows the in-situ FBG temperature sensor design used in this work. The probe length is 1.5 m and it contains a single 5 mm FBG head imprinted in a polyimide coated fibre. The FBG head bandwidth is $\approx$0.374 nm and its reflectivity $\approx$88%. A section of the sensing fibre containing the FBG head is packaged in a PEEK capillary while the remainder of the optic cable is tubed in Teflon for protective purposes. The outer diameter of the utilised PEEK capillary was chosen as 0.8 mm. This was done to provide a relatively close match to the 0.56 mm diameter size of the examined stator winding's copper wire and therefore facilitate easier placement and more effective thermal sensing performance of the sensor package within the random wound stator winding structure [37], [40]. The PEEK capillary wall thickness was chosen to be 0.1 mm to yield a low conduction thermal resistance and hence enhance the sensor response [40].

Two aspects of internal sensing location were considered in sensor design for the winding slot sections: the sensor axial and radial position. The radial position requirements dictated sensor placement in the cross-sectional centre point of the slot section, where the thermal hot spot is located; this is enabled by appropriate PEEK packaging of the FBG sensor, discussed earlier in this section. Regarding axial sensing position the proposed scheme is designed to enable arbitrary sensor positioning. To this end the packaging capillary length was designed to be closely similar to the examined machine's winding axial length; this enabled the packaging capillary to house the entire fibre section containing the FBG sensing head that is implanted in the winding slot region, starting from the NDE-winding through the slot section to DE-winding, as illustrated in Fig. 5(b). The sensing fibre is kept loose within packaging. This design allows for positioning of the FBG sensing head at any desired point

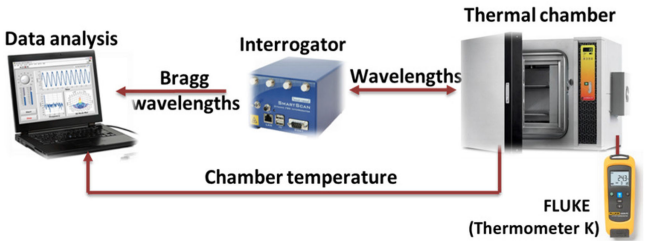

Fig. 6. Experimental system for FBG sensor calibration tests.

along the axial length of the winding slot section. As the purpose of this study is to examine the performance of the proposed monitoring scheme and considering the size of the commercial test machine imposes relatively minor thermal differences in the slot axial direction, the FBG head was placed in the centre of the core axial length as shown in Fig. 5(b). The packaged sensors in the end-winding sections were embedded in the end-winding section cross-sectional centre point. This enabled practical monitoring of internal temperature of different winding sections (i.e., slot and end winding hot spots). Combined with the multiplexing feature of FBG sensors this design can allow different distributed thermal configurations to be established: a single fibre with multiple FBGs can monitor the axial length of the winding including slot and end-winding sections.

C. In-Situ FBG Temperature Sensor Calibration

The interpretation of the FBG sensor reflected Bragg wavelength to temperature readings first requires a sensor calibration test to obtain the required temperature-wavelength fit curve [40]. The experimental setup for calibration of the described FBG sensor design is shown in Fig. 6. A controlled thermal chamber was used to expose the sensors to a desired, controlled, steady-state thermal excitation level. The reference temperature within the thermal chamber was read by the chamber proprietary thermal sensors and a type K TC sensor placed inside the chamber in close proximity to the FBG sensors under calibration. The FBG sensors were illuminated by a commercial SmartScan interrogator system enabling dynamic measurement of reflected wavelengths.

Calibration tests were performed in the temperature range of 20 to 160 °C to match the rated thermal range of the class F insulated motor windings. The temperature was regulated by the chamber controller in the tests in a rising sequence of 20 °C steps. At each step the temperature was held constant for a time period sufficient to ensure the thermal equilibrium is achieved before thermal measurements were taken. The FBG reflected wavelength and the chamber temperature were recorded at each evaluated thermal equilibrium in the investigated temperature range. The calibration test data for the four FBG sensors used in this work are presented in Fig. 7 and show a close-to-linear temperature-wavelength dependency. A second order polynomial fit curve was calculated from the obtained data for each FBG to enable accurate conversion of the monitored reflected wavelength shift to temperature readings in further tests [39].

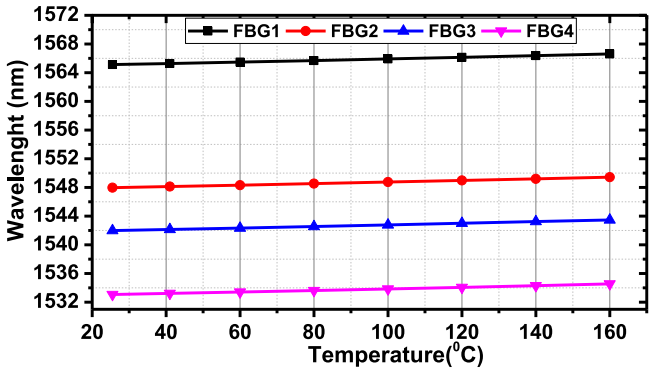

Fig. 7. Sensor calibration test data.

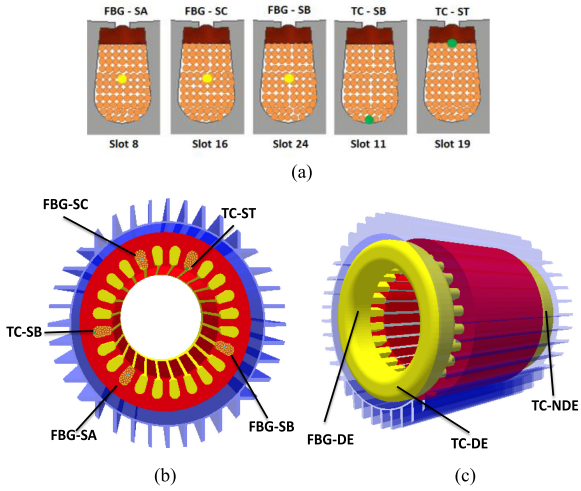

Fig. 8. Temperature sensor positions in the tested motor. (a) Sensor positions in slot sections. (b) Slot section sensor arrangement. (c) End-winding sensor arrangement.

IV. Induction Machine Hot Spot Monitoring System Experimental Test Rig Description

This section describes the design and implementation of the winding hot spot monitoring experimental system. The proposed on-line monitoring scheme was established by installing a number of FBG probe designs discussed in Section III into the test induction machine specified in Table I. For the purpose of embedding the sensors in the target positions, the motor stator winding was stripped and rewound.

Fig. 8 illustrates the embedded thermal sensor locations in the test machine. These were chosen to include both slot and end-winding portion hot spots of the stator windings, as discussed in Section II. To this end, three FBG sensors were embedded between copper conductors in the slot centre of three different slots, each slot containing a different phase winding (one FBG fitted per phase, referred to as FBG-SA, FBG-SB and FBG-SC in further text, respectively), as illustrated in Fig. 8(a). The three FBGs were pitched by 8 slots to enable a uniform thermal sensing distribution within the examined motor geometry, as shown in Fig. 8(b). An additional, fourth, FBG sensor (FBG-DE in further text) was embedded in the motor drive end end-winding section, shown in Fig. 8(c).

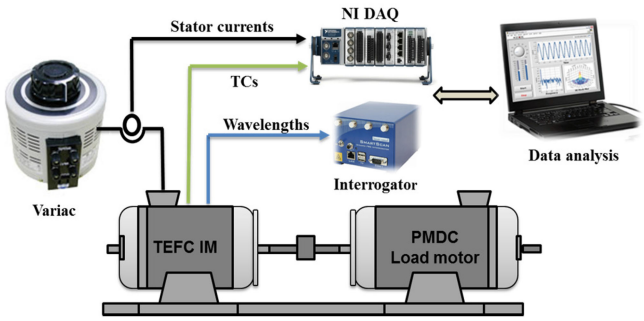

Fig. 9. Experimental test rig for TEFC on-line temperature monitoring.

To ensure the installed sensors are approximately positioned in the coil centre the following installation procedure was followed [37]–[40]. First the packaging capillaries were embedded within the slot structure during the rewind process. This was achieved by winding half of a relevant coil section and inserting it in its respective slot/end winding position, before fitting the packaging capillary in the coil centre location and winding the remainder of the coil. Once the winding process was completed and the windings impregnated (dip impregnation) the FBG sensing fibres were loosely inserted into the installed PEEK capillaries. This process enables in-situ hot spot sensing in positions of interest and offers an advantage of avoiding the undesirable exposure of the fragile sensing fibre to mechanical stress during the wind and impregnation process. Another key practical advantage is that the sensing fibre is made accessible for replacement, re-positioning and/or re-calibration, which is not the case with conventional thermal sensors [50].

To benchmark the in-situ FBG sensing thermal system performance a number of type K thermocouples were embedded in the stator windings as shown in Fig. 8. Two TCs were embedded in the end-windings: one in the drive end (TC-DE) to benchmark the FBG-DE performance and the other in the non-drive end (TC-NDE) to validate the obtained results. Another two TCs were embedded between the coil surface and the slot wall insulation, one in the bottom of the slot (TC-SB) and the other in the top of the slot under the slot wedge (TC-ST). The TCs positions where chosen in accordance with the IEC 60034-1 standard [23].

The test rig used to examine the on-line performance of the proposed in-situ thermal monitoring system is illustrated in Fig. 9. The rig contains the prototype FBG sensor embedded induction motor coupled to a PMDC load machine whose armature current is regulated using a controllable resistive load bank. The induction motor was supplied directly from the grid via a variable transformer in the tests. Its currents were measured using LEM-LA25 Hall effect current transducers whose output was monitored via an NI 9205 DAQ and conditioned on a personal computer in a LabView VI routine. TC outputs were acquired and conditioned by a thermocouple input module NI9211 DAQ. The FBG sensors were illuminated by a commercial multi-channel Smart Fibres SmartScan04 interrogator unit; the monitored FBG wavelengths were processed using the LabView based SmartSoft software [30].

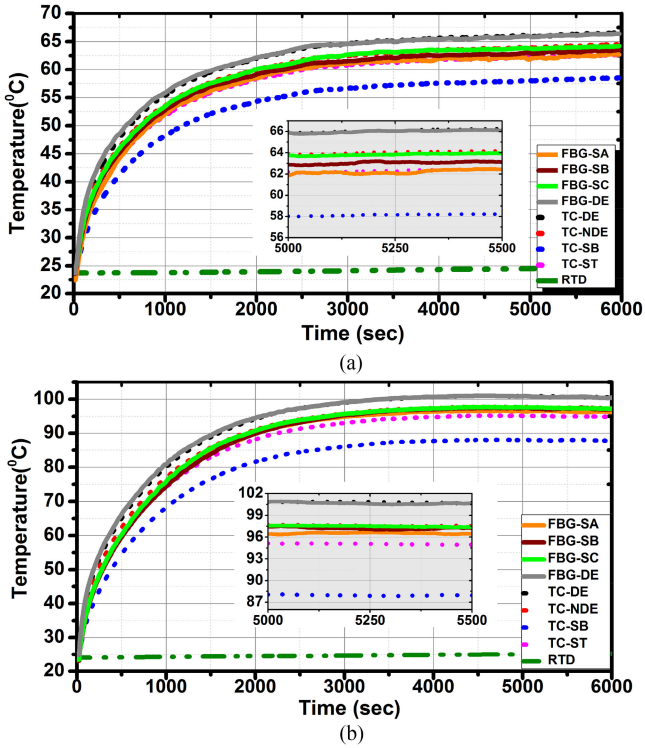

Fig. 10. Stator winding temperature measured by in situ FBG and TC sensors during running duty cycle S1 operation: (a) no-load. (b) full-load.

V. Experimental Results

The on-line hot spot monitoring performance of the proposed in-situ FBG sensing system was evaluated in extensive thermal tests on the prototype FBG embedded motor. This section presents the winding internal thermal readings obtained in a range of typical dynamic thermal cycle tests performed on the laboratory test rig. The applied thermal cycles were defined based on the IEC 60034-1 standard for rating and performance of rotating machines [23]. The thermal characteristics of the examined motor design have been considered in order to enhance the interpretation of the obtained measurements.

A. Continuous Running Duty Operation

A significant proportion of TEFC induction motors in modern industrial applications are S1 duty rated. The S1 duty rating specifies continuous machine operation under a constant load, maintained for a time period sufficient to allow the machine to reach a thermal equilibrium within its nominal rating [23].

The proposed monitoring system's performance was first examined for test motor operation in a number of S1 continuous duty cycles. To this end a series of S1 cycles at different load levels were applied on the test motor, ranging from no-load to nominal load in increments of 25% (i.e., 0%, 25%, 50%, 75% and 100% load). The thermal measurements obtained by in-situ FBG and TC sensors at 0% and 100% load S1 duty cycles are shown in Fig. 10 for illustrative purposes. The winding temperature rise measured at thermal equilibrium for all considered S1 duty cycles is shown in Fig. 11; this was calculated by averaging

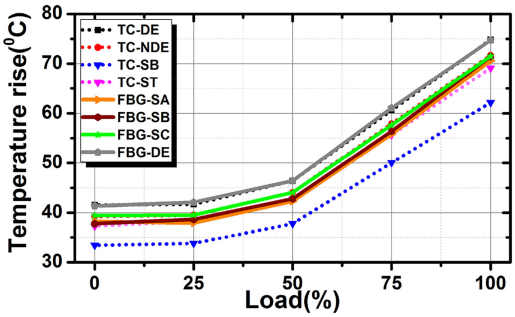

Fig. 11. Measured S1 duty cycle steady-state temperature rise versus load.

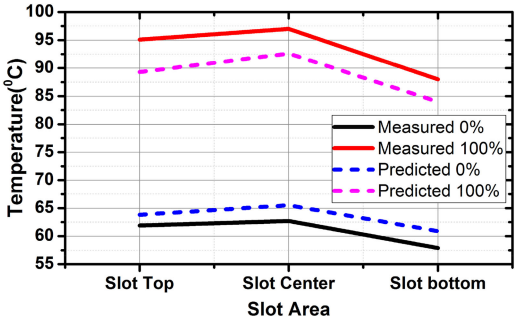

Fig. 12. Temperature gradients measured within the slot area.

the winding temperature measurement referred to the measured ambient temperature during a 15 min steady-state period of each examined duty cycle. The ambient temperature was measured by an RTD sensor connected to an RTD input module NI 9217 DAQ. The RTD was placed at shaft height and at one meter distance from the motor as prescribed in [23]. The ambient temperature measured in the tests is shown in Fig. 10 for illustration purposes.

A variety of information about the FBG sensing system performance and the motor thermal characteristics can be extracted from the presented measurements. Firstly, it is evident from Fig. 10 that the average internal winding temperature exhibits a relatively large increase of ≈34 °C, from ≈64 °C at no-load to ≈98 °C at full-load. This can be explained by the examined motor's standard efficiency class (IE1) design, expected to exhibit a significant increase in losses, and stator winding loss in particular, with increase in load [51]. The thermal rise is further enhanced by the relative degradation of the cooling process (shaft mounted fan) due to a relatively significant rotor speed reduction at full-load, resulting from the large nominal slip (≈8%) of the tested motor design.

The maximum winding temperatures are recorded at full-load: ≈100 °C in the drive end end-winding measured by FBG-DE and confirmed by TC-DE, and an average of ≈96 °C in the slot section measured by FBG-SA, FBG-SB and FBG-SC. These hot spot readings are ≈50 °C below the maximum allowable temperature of the examined motor (155 °C). The readings conform to the class F insulation and class B temperature rise ratings of the investigated motor design, commonly used by manufacturers to lengthen the insulation life by lowering winding temperature at rated load [52]. This is illustrated in Fig. 11 by the measured hot spot temperature rise at full-load of ≈75 °C, ≈5 °C lower than the permissible temperature rise of class B rated motors of 80 °C. The temperature rise measured for no-load to 50% load conditions is approximately half of that observed for full-load operation, as is expected for an IE1 class motor [51].

The data in Figs. 10 and 11 allow for another important observation relating to the increase in the difference between thermal readings reported by sensors embedded at different locations with the change in motor load. The difference between the drive end end-winding temperature (FBG-DE, TC-DE) and the slot bottom temperature (TC-SB) for example is seen to increase from ≈7 °C at no-load to ≈13 °C at full-load. This clearly demonstrates the importance of thermal sensing in appropriate locations for accurate tracking of the highest stator winding temperature. The FBG hot spot thermal measurements and those obtained by TC sensors are seen to be in good agreement with the optimised thermal model predictions shown in Figs. 3 and 4. As expected, the FBGs placed in the slot centre report higher thermal readings when compared to the TCs placed in contact with coil slot section surface. At no-load, the TC sensors installed on the top (TC-ST in Fig. 8) and the bottom of the coil slot section (TC-SB in Fig. 8) report a temperature that is ≈0.9 °C and ≈3.6 °C lower than that recorded by the FBGs in the slot centre, respectively. The difference between the TC-SB and TC-ST sensor readings and those of slot centre placed FBGs increases with load and is measured as ≈9 °C and ≈2 °C at full-load, respectively.

The temperatures within the slot area measured by FBGs in the slot centre and TCs at slot top and bottom (TC-SB and TC-ST), and predicted by the FE thermal model in Fig. 4 are shown in Fig. 12 for the lowest and the highest measured temperature gradient (i.e., for 0% and 100% load). The data indicate that the temperature gradient within the slot area increases with load for the investigated motor design. The heat generated within the slot increases with the square of the winding current which in turn rises with load; the heat dissipation path in the slot area on the other hand is largely defined by the slot fill factor, winding impregnation and the slot liner design. Therefore, for operation at full-load the heat generation rate within the slot increases considerably with respect to the attainable slot heat dissipation rate, resulting in a large temperature gradient and a high thermal hot spot in the slot centre. The observed difference between thermal measurements in the slot hot spot point (i.e., centre) and the slot top and bottom points is seen to change with load and is an artefact of the heat dissipation process. The slot bottom is affected by the proximity of the core yoke which exhibits a largely load independent loss mechanism and therefore provides a relatively effective cooling path between the slot conductors and the ambient. Conversely, the top of the slot is affected by the air gap and rotor temperatures which generally increase with load [52]. This is demonstrated by the difference between the thermal readings in the slot top and bottom positions, which increases from ≈3.5 °C at no-load to ≈7 °C at full-load. The experimental data in Fig. 12 clearly illustrate the advantage of thermal sensing in the slot centre position, where the highest thermal stress within the slot area is located.

The drive end end-winding temperature was measured to be ≈2.2 °C higher at no-load and ≈3.6 °C higher at full-

load, than the slot hot spot temperature (FBG-SA, FBG-SB, FBG-SC). This difference arises due to the slow end-winding cooling process, largely based on convective heat transfer; the distance between the motor drive end and its cooling fan is another influencing factor, as it results in the air inflow reaching the end cap being significantly hotter than that at the cooling fan. It is interesting to observe that the measured ambient temperature increases by up to ≈3 °C in performed tests as a result of the heat dissipated in the surrounding ambient by the tested induction motor as well as its load motor with the resistance bank. The observed thermal increase can be higher in applications where the surrounding ambient consists of heat sources in close proximity to the motor that can be drawn back by the cooling air inlets and increase the motor temperature [52].

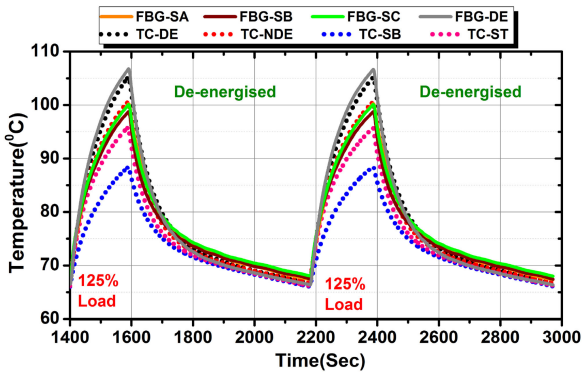

Fig. 13. Measured temperature under intermittent duty cycle S3.

B. Periodic Running Duty Operation

In many industrial applications TEFC motors are operated in variable-load periodic duties. These dynamic operating conditions can pose a risk of giving rise to motor internal temperatures increase beyond permissible levels and thus endanger its integrity. The current industrial thermal protection systems for electric motors used to prevent overheating in these conditions are not fully effective [16]. It is challenging for existing thermal relays to accurately determine the motor's thermal characteristic under different operating conditions as they are mostly designed based on a single thermal time constant. As a result these are often too conservative, resulting in unnecessary stoppage, or alternatively can incorrectly interpret existing thermal conditions and consequently fail to react, resulting in significant overheating [18]. For effective utilisation and protection of motors operated in periodic running duty applications the accuracy of internal winding temperature monitoring is essential.

This section examines the proposed system's performance when used for on-line thermal monitoring of the test motor operating under intermittent periodic duty S3 and continuous–operating periodic duty S6, as defined by IEC 60034-1 [23]. The applied cycles' period and duration factor were controlled to ensure that the motor's highest hot spot temperature rise rate reaches but does not exceed the maximum permissible temperature rise rate for its design class.

1) Duty Type S3 - Intermittent Periodic Duty: The S3 duty type is identified as a sequence of identical duty cycles, each including a time of operation at constant load and a time de-energised and at rest, where the starting current is such that it does not significantly affect the temperature rise [23]. An S3 23% cyclic duration factor was applied to the examined motor for the purpose of this test; this was achieved by periodically applying 125% of rated load for a duration of 3 min followed by a 10 min de-energised period. The dynamic thermal measurements obtained by the embedded FBG and TC sensors are shown in Fig. 13.

The maximum temperature is recorded at completion of the constant load period and is measured in the drive end end-winding at ≈106 °C, which is equal to the sum of the measured motor temperature rise of ≈80 °C and the measured ambient temperature of ≈26 °C. The embedded thermal sensors report different temperature rates of change in heating and cooling conditions. The FBG sensors embedded in the slot centre show higher thermal readings and lower heating thermal time constants when compared to those obtained by TC sensors attached to the coil surface. In the examined S3 duty type the test motor is periodically de-energised for a period of time after a period of over loading. A sufficient cooling period duration is therefore highly desirable in this duty, to prevent the motor from overheating when starting up in the following cycle. Things are further complicated by the fact that the TEFC motor cooling characteristic significantly changes based on whether it is energised: the cooling mechanism changes from forced and natural convection heat transfer in an energised motor, to only natural convection heat transfer in a de-energised motor. The latter heat transfer mechanism is slower and thus results in a larger cooling thermal time constant, as observed in the hot spot thermal measurements in Fig. 13. Accurate tracking of hot spot winding temperature is thus essential to reliably identify the time required for the motor to cool down to a temperature sufficiently low to allow its safe and effective re-energisation.

2) Duty Type S6–Continuous Operation Periodic Duty: The continuous operating periodic duty type S6 is specified as a sequence of identical duty cycles: each cycle consists of a period of operation at constant load and a period of operation at no-load; at no time is the motor de-energised, at rest or reaches a thermal equilibrium [23]. In this experiment, an S6 duty type with a period of 20 min and a cyclic duration factor of 50% was applied to the test motor. In each cycle the motor is loaded at 125% of rated load for a 10 min period and then run under no-load for the remainder of the cycle. The recorded temperature readings obtained by the embedded FBG and TC sensors are shown in Fig. 14. The highest temperature was measured to be ≈100 °C in the drive end end-winding. The ambient temperature was measured as ≈25.2 °C during the experiment. The studied S6 cycle could therefore be deemed to be safe to apply on the examined motor as the highest measured temperature is lower than the permissible temperature for the motor insulation class and the highest measured thermal rise rate (≈75 °C) is lower than the designed class B temperature rise. However, a small increase in the examined cyclic duration factor can result in temperature rise beyond that permissible for the tested motor design.

3) Discussion: The presented thermal dynamic profiles demonstrate the capability of the in-situ FBG sensing system to

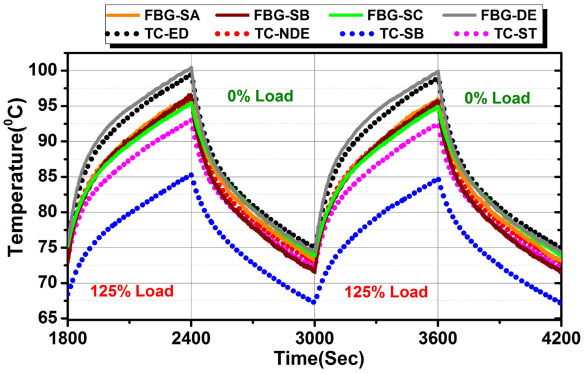

Fig. 14. Measured temperature under continuous operation duty cycle S6.

provide effective on–line tracking of internal winding temperature in typical periodic running duty applications. The obtained winding hot spot measurements clearly show the different heating and cooling time constants and report a noticeable difference between individual measurements during the examined duty cycles. Therefore, relying on the average winding temperature in these conditions, such as would be provided by a resistance estimator technique, is not adequate to fully protect the motor from overheating, as the difference between average winding temperature and a localised hot spot can be high. This clearly illustrates the limitations in motor thermal protection by conventional thermal relays based on single time constant recognition and the advantages that the proposed monitoring scheme can provide in this regard.

VI. Conclusion

The paper reports a new and robust technique for on-line thermal hot spot monitoring in low voltage machinery random wound windings using FBG sensing technology. The proposed scheme has been implemented and its performance examined and validated on a mains-fed TEFC squirrel cage motor.

The proposed scheme utilises electrically non-conductive and EMI immune, power passive, fibre optic sensors that are particularly suitable for embedded application in random wound coils in a variety of machine sizes, ratings and applications. The reported in-situ monitoring network design enables sensor in-situ accessibility for replacement, repositioning or recalibration which is not possible with conventional sensing techniques, and provides a versatile and safety critical monitoring platform that can be expanded to achieve further embedded distributed thermal sensing capability.

The reported scheme was applied to perform thermal measurements on a prototype mains-fed induction motor operating in a number of continuous and periodic running duty cycles identified by the IEC standards. Where possible, the measured temperatures were cross correlated with measurements obtained by conventional TC sensors and with temperatures predicted by a thermal model of the test motor, which was initially used to inform the general thermal monitoring scheme design. The obtained experimental data illustrate the advantages of the proposed in-situ sensing scheme in delivering robust and effective on-line thermal sensing in thermal hot spot positions internal to the winding structure, where the highest thermal stress within the slot and end-winding areas is located.

The reported thermal analysis enables an enhanced understanding of actual motor thermal conditions during on-line operation and could be used for enhancing the utilisation and protection of electric motors in future safety critical industrial applications. A particularly pertinent condition in this regard is motor operation in different dynamic cycles such as those examined in this work, where the proposed technique clearly reports different hot-spot thermal time constants and illustrates the limitations of motor monitoring and protection systems based on application of a pre-defined single thermal time constant. Furthermore, the accurate tracking of the actual winding hot spot temperature is essential to identify the required time of motor de-loading to enable sufficient cooling in dynamic duty cycles, where any inaccuracies in thermal monitoring will either lead to a reduction of motor effective operation time or, more critically, a reduction of its life time through thermal overload.

The reported study demonstrates the potential of the proposed in-situ thermal sensing scheme to enable monitoring and recognition of winding thermal conditions in arbitrary internal positions, thus enabling a much improved awareness of key thermal parameters in operating low voltage induction machinery that would be exceptionally challenging and impractical to achieve with conventional monitoring techniques.

References

[1] W. Cao, B. C. Mecrow, G. J. Atkinson, J. W. Bennett, and D. J. Atkinson, "Overview of electric motor technologies used for more electric aircraft (MEA)," *IEEE Trans. Ind. Electron.*, vol. 59, no. 9, pp. 3523–3531, Sep. 2012.

[2] K. Fischer, F. Besnard, and L. Bertling, "Reliability-centered maintenance for wind turbines based on statistical analysis and practical experience," *IEEE Trans. Energy Convers.*, vol. 27, no. 1, pp. 184–195, Mar. 2012.

[3] J. de Santiago *et al.*, "Electrical motor drivelines in commercial all-electric vehicles: A review," *IEEE Trans. Veh. Technol.*, vol. 61, no. 2, pp. 475–484, Feb. 2012.

[4] M. O. Sonnaillon, G. Bisheimer, C. D. Angelo, and G. O. García, "Online sensorless induction motor temperature monitoring," *IEEE Trans. Energy Convers.*, vol. 25, no. 2, pp. 273–280, Jun. 2010.

[5] N. Z. Popov, S. N. Vukosavic, and E. Levi, "Motor temperature monitoring based on impedance estimation at PWM frequencies," *IEEE Trans. Energy Convers.*, vol. 29, no. 1, pp. 215–223, Mar. 2014.

[6] D. Milić Saša, A. D. Žigić, and M. M. Ponjavić, "Online temperature monitoring, fault detection, and a novel heat run test of a water-cooled rotor of a hydrogenerator," *IEEE Trans. Energy Convers.*, vol. 28, no. 3, pp. 698–706, Sep. 2013.

[7] H. Zhang, "Online thermal monitoring models for induction machines," *IEEE Trans. Energy Convers.*, vol. 30, no. 4, pp. 1279–1287, Dec. 2015.

[8] "Electric machines roadmap," Advanced Propulsion Centre, UK Automotive Council, Coventry, U.K., 2017.

[9] S. Rogers and S. Boyd, "Overview of the DOE VTO electric drive technologies R&D program," US Dept. Energy Veh. Technol. Office, Washington, DC, USA, Jun. 2016.

[10] S. Arfat, G. S. Yadava, and B. Singh, "A review of stator fault monitoring techniques of induction motors," *IEEE Trans. Energy Convers.*, vol. 20, no. 1, pp. 106–114, Mar. 2005.

[11] S.-B. Lee, T. G. Habetler, R. G. Harley, and D. J. Gritter, "An evaluation of model-based stator resistance estimation for induction motor stator winding temperature monitoring," *IEEE Trans. Energy Convers.*, vol. 17, no. 1, pp. 7–15, Mar. 2002.

[12] A. H. Bonnett, "Operating temperature considerations and performance characteristics for IEEE 841 motors," *IEEE Trans. Ind. Appl.*, vol. 37, no. 1, pp. 1120–1131, Jul./Aug. 2001.

[13] H. Jonathan, A. C. Malloy, R. Martinez-Botas, and M. Lampérth, "Online monitoring of electromagnetic losses in an electric motor indirectly

through temperature measurement," *IEEE Trans. Energy Convers.*, vol. 31, no. 4, pp. 1347–1355, Dec. 2016.
[14] *NEMA Motor-Generator Standard*, Standard MG-1-2014, 2014.
[15] D. Reimert, *Protective Relaying for Power Generation Systems*. Boca Raton, FL, USA: CRC Press, 2005, ch. 16, sec. 10, pp. 497–498.
[16] M. A. Valenzuela and P. Reyes, "Simple and reliable model for the thermal protection of variable-speed self-ventilated induction motor drives," *IEEE Trans. Ind. Appl.*, vol. 46, no. 2, pp. 770–778, Mar./Apr. 2010.
[17] Z. Gao, T. G. Habetler, R. G. Harley, and R. S. Colby, "A sensorless adaptive stator winding temperature estimator for mains-fed induction machines with continuous-operation periodic duty cycles," *IEEE Trans. Ind. Appl.*, vol. 44, no. 5, pp. 1533–1542, Sep./Oct. 2008.
[18] P. Zhang, B. Lu, and T. G. Habetler, "An active stator temperature estimation technique for thermal protection of inverter-fed induction motors with considerations of impaired cooling detection," *IEEE Trans. Ind. Appl.*, vol. 46, no. 5, pp. 1873–1881, Sep./Oct. 2010.
[19] Z. Lazarevic, R. Radosavljevic, and P. Osmokrovic, "A novel approach for temperature estimation in squirrel-cage induction motor without sensors," *IEEE Trans. Instrum. Meas.*, vol. 48, no. 3, pp. 753–757, Jun. 1999.
[20] P. Tavner, Li Ran, and J. Penman, *Condition Monitoring of Rotating Electrical Machines (IET Power and Energy Series)*. London, U.K.: Inst. Eng. Technol., 2008.
[21] P. B. Reddy, A. M. El-Refaie, K. K. Huh, J. K. Tangudu, and T. M. Jahns, "Comparison of interior and surface PM machines equipped with fractional-slot concentrated windings for hybrid traction applications," *IEEE Trans. Energy Convers.*, vol. 27, no. 3, pp. 593–602, Sep. 2012.
[22] N. Z. Popov and S. N. Vukosavic, "Estimator of the rotor temperature of induction machine based on terminal voltages and currents," *IEEE Trans. Energy Convers.*, vol. 32, no. 1, pp. 155–163, Mar. 2017.
[23] *Rotating Electrical Machines - Part 1: Rating and Performance*, IEC Standard 60034-1:2010, 2010.
[24] N. M. Theune et al., "Investigation of stator coil and lead temperatures on high voltage inside large power generators via use of fiber Bragg gratings," in *Proc. IEEE Sens.*, 2002, vol. 2, pp. 1603–1607.
[25] F. Marignetti *et al.*, "Fiber Bragg grating sensor for electric field measurement in the end windings of high-voltage electric machines," *IEEE Trans. Ind. Electron.*, vol. 63, no. 5, pp. 2796–2802, May 2016.
[26] D. S. Vilchis-Rodriguez, S. Djurović, P. Kung, M. I. Comanici, and A. C. Smith, "Investigation of induction generator wide band vibration monitoring using fibre Bragg grating accelerometers," in *Proc. Int. Conf. Electr. Mach.*, 2014, pp. 1772–1778.
[27] K. M. Sousa, U. J. Dreyer, C. Martelli, and J. C. C. da Silva, "Dynamic eccentricity induced in induction motor detected by optical fiber Bragg grating strain sensors," *IEEE Sens. J.*, vol. 16, no. 12, pp. 4786–4792, Jun. 2016.
[28] W. Ecke and K. Schröder, "Fiber Bragg grating sensor system for operational load monitoring of wind turbine blades," *Proc. SPIE*, vol. 6933, 2008, Art. no. 69330I.
[29] Z. Gao *et al.*, "Active monitoring and vibration control of smart structure aircraft based on FBG sensors and PZT actuators," *Aerosp. Sci. Technol.*, vol. 63, pp. 101–109, 2017.
[30] Smartfibres.com., "Smart fibres | Pioneering optical fibre sensing," 2017. [Online]. Available: http://www.smartfibres.com.
[31] N. Haramoni, A. S. Paterno, J. C. C. Silva, and H. J. Kalinowski, "Hybrid wavelength-time-domain interrogation system for multiplexed fiber Bragg sensors using a strain-tuned erbium-doped fiber laser," *IEEE Sens. J.*, vol. 8, no. 7, pp. 1061–1066, Jul. 2008.
[32] M. M. Werneck, R. C. da Silva Barros Allil, and B. A. Ribeiro, "Calibration and operation of a fibre Bragg grating temperature sensing system in a grid-connected hydrogenerator," *IET Sci., Meas. Technol.*, vol. 7, no. 1, pp. 59–68, 2013.
[33] K. D. M. Sousa, A. A. Hafner, H. J. Kalinowski, and J. C. C. da Silva, "Determination of temperature dynamics and mechanical and stator losses relationships in a three-phase induction motor using fiber Bragg grating sensors," *IEEE Sens. J.*, vol. 12, no. 10, pp. 3054–3061, Oct. 2012.
[34] J. M. Corres, J. Bravo, F. J. Arregui, and I. R. Matias, "Unbalance and harmonics detection in induction motors using an optical fiber sensor," *IEEE Sens. J.*, vol. 6, no. 3, pp. 605–612, Jun. 2006.
[35] R. P. Linessio, K. D. M. Sousa, T. da Silva, C. A. Bavastri, P. F. D. C. Antunes, and J. C. C. da Silva, "Induction motors vibration monitoring using a biaxial optical fiber accelerometer," *IEEE Sens. J.*, vol. 16, no. 22, pp. 8075–8082, Nov. 2016.
[36] *IEEE Recommended Practice for Thermal Cycle Testing of Form-Wound Stator Bars and Coils for Large Rotating Machines - Redline*, IEEE Standard 1310-2012 (Revision of IEEE Standard 1310-1996), May 2012.
[37] A. Mohammad and S. Djurović, "Evaluation of fiber-optic sensing performance for embedded thermal monitoring of electric machinery wound components," in *Proc. 5th Mediterranean Conf. Embedded Comput.*, 2016, pp. 72–76.
[38] A. Mohammed, S. Djurović, A. C. Smith, and K. Tshiloz, "FBG sensing for hot spot thermal monitoring in electric machinery random wound components," in *Proc. 22nd Int. Conf. Electr. Mach.*, Lausanne, Switzerland, 2016, pp. 2266–2272.
[39] A. Mohammed and S. Djurović, "FBG array sensor use for distributed internal thermal monitoring in low voltage random wound coils," in *Proc. 6th Mediterranean Conf. Embedded Comput.*, 2017, pp. 1–4.
[40] A. Mohammed and S. Djurović, "FBG thermal sensing features for hot spot monitoring in random wound electric machine coils," *IEEE Sens. J.*, vol. 17, no. 10, pp. 3058–3067, May 2017.
[41] Motor Design, "Motor-CAD Software by motor design - EMag, Therm and Lab," 2017. [Online]. Available: https://www.motor-design.com/motor-cad-software.
[42] D. A. Staton and A. Cavagnino, "Stator winding thermal conductivity evaluation: An industrial production assessment," *IEEE Trans. Ind. Electron.*, vol. 52, no. 5, pp. 3509–3516, Oct. 2016.
[43] D. A. Staton and A. Cavagnino, "Winding design for minimum power loss and low cost," *IEEE Trans. Ind. Electron.*, vol. 55, no. 10, pp. 3509–3516, Oct. 2015.
[44] D. Staton, A. Boglietti, and A. Cavagnino, "Solving the more difficult aspects of electric motor thermal analysis in small and medium size industrial induction motors," *IEEE Trans. Energy Convers.*, vol. 20, no. 3, pp. 620–628, Sep. 2005.
[45] *IEEE Standard Test Procedure for Polyphase Induction Motors and Generators*, IEEE Standard 112-2004 (Revision of IEEE Standard 112-1996), 2004.
[46] A. Boglietti, A. Cavagnino, M. Lazzari, and A. Pastorelli, "A simplified thermal model for variable speed self-cooled industrial induction motor," in *Proc. Conf. Rec. IEEE Ind. Appl. Conf. 37th IAS Annu. Meeting*, Pittsburgh, PA, USA, 2002, vol. 2, pp. 723–730.
[47] Y. J. Rao, "In-fibre Bragg grating sensors," *Meas. Sci. Technol.*, vol. 8, no. 4, pp. 355–375, 1997.
[48] M. Reddy, S. Kamineni, and V. Rao Pachava, "Characterization of encapsulating materials for fiber Bragg grating-based temperature sensors," *Fiber Integr. Opt.*, vol. 33, no. 4, pp. 325–335, 2014.
[49] A. D. Kersey, M. A. Davis, H. J. Patrick, and M. Leblane, "Fiber grating sensors," *J. Lightw. Technol.*, vol. 15, no. 8, pp. 1442–1463, Aug. 1997.
[50] *IEEE Recommended Practice for General Principles of Temperature Measurement as Applied to Electrical Apparatus*, IEEE Standard 119-1974, 1974.
[51] F. J. T. E. Ferreira, B. Leprettre, and A. T. de Almeida, "Comparison of protection requirements in IE2-, IE3-, and IE4-class motors," *IEEE Trans. Ind. Appl.*, vol. 52, no. 4, pp. 3603–3610, Jul./Aug. 2016.
[52] A. H. Bonnett, "Operating temperature considerations and performance characteristics for IEEE 841 motors," *IEEE Trans. Ind. Appl.*, vol. 37, no. 1, pp. 1120–1131, Jul./Aug. 2001.

Anees Mohammed received the M.Sc. degree in electrical power engineering from the University of Newcastle, Newcastle upon Tyne, U.K., in 2010. He is currently working toward the Ph.D. degree in electrical and electronic engineering at the University of Manchester, Manchester, U.K. He spent four years as an Assistant Lecturer with Benghazi University, Benghazi, Libya. His research interests include electric machines, drives, and condition monitoring.

Siniša Djurović (M'09) received the Dipl. Ing. degree in electrical engineering from the University of Montenegro, Podgorica, Montenegro, in 2002, and the Ph.D. degree from the University of Manchester, Manchester, U.K., in 2007. He is a Senior Lecturer with the Power Conversion Group, University of Manchester. His research interests include the area of operation, design, monitoring, and diagnostics of electric machines and drives.